

Optical Near-Field Microscopy of Light Focusing through a Photonic Crystal Flat Lens

Nathalie Fabre,¹ Loïc Lalouat,² Benoit Cluzel,² Xavier Mélique,¹ Didier Lippens,¹
Frédérique de Fornel,² and Olivier Vanbésien¹

¹*Institut d'Electronique, de Microélectronique et de Nanotechnologie (IEMN), UMR CNRS 8520, Université des Sciences et Technologies de Lille, Cité Scientifique, BP 60069, F-59652 Villeneuve d'Ascq Cedex, France*
²*Groupe d'Optique de Champ Proche, Institut Carnot de Bourgogne (ICB), UMR CNRS 5209, Université de Bourgogne, 9, avenue A. Savary, BP 47870, 21078 Dijon, France*

(Received 13 March 2008; revised manuscript received 24 June 2008; published 11 August 2008)

We report here the direct observation by using a scanning near-field microscopy technique of the light focusing through a photonic crystal flat lens designed and fabricated to operate at optical frequencies. The lens is fabricated using a III-V semiconductor slab, and we directly visualize the propagation of the electromagnetic waves by using a scanning near-field optical microscope. We directly evidence spatially, as well as spectrally, the focusing operating regime of the lens. At last, in light of the experimental scanning near-field optical microscope pictures, we discuss the lens ability to focus light at a subwavelength scale.

DOI: [10.1103/PhysRevLett.101.073901](https://doi.org/10.1103/PhysRevLett.101.073901)

PACS numbers: 42.70.Qs, 07.79.Fc, 42.82.-m

Since the pioneering works of Veselago [1] and Pendry [2] dedicated to the focusing properties of a slab with a negative refractive index, many proposals have been done in the field of metamaterials to demonstrate this effect. As the negative refraction requires artificial materials patterned on a subwavelength scale [3], the very first trials to demonstrate this phenomenon were performed at microwave frequencies. In this field, a resolution of $\lambda/8$ at 3.8 GHz was reported by using a metallic metamaterial [4], opening the route towards promising “superlenses” which overcome the Rayleigh limit. At optical frequencies, metals become lossy, and the challenge appears more difficult. To overcome this difficulty, the use of purely dielectric structures such as semiconductor photonic crystals (PCs) is intensively investigated. In this case, an *effective* negative index of refraction of $n = -1$, instead of a permeability (ϵ) and permittivity (μ) both equal to -1 , can be achieved by controlling the Bloch wave dispersion. However, the ability of such a photonic crystal to act as a superlens remains controversial [5,6].

At optical frequencies, if the two-dimensional photonic crystal (2DPC) ability to exhibit a negative refraction [7,8] and a focusing regime [9,10] has been indirectly evidenced in the optical far field, no direct superlens demonstration has been reported so far since the phenomenon relies on the properties of evanescent waves [2,11], which exist only in the optical near field. Consequently, the scanning near-field optical microscopy (SNOM) techniques are particularly relevant to the analysis of such nanostructures. In this work, we report the SNOM experimental observations of the lensing phenomenon by directly addressing at telecommunication frequency ($\lambda = 1.55 \mu\text{m}$) the electromagnetic field distribution in a photonic crystal flat lens. The negative refraction regime that leads to the light refocalization of a point source is directly visualized spatially as well as spectrally. Finally, we estimate the resolution of the lens in

light of the experimental results and discuss the ability of the reported lens to overcome the classical limitation in terms of subwavelength resolution.

First, in order to define the optogeometrical parameters of the 2DPC flat lens, we show in Fig. 1 the band diagram and the isofrequency contours of a triangular lattice of air holes etched in the semiconductor heterostructure (InP/GaInAsP/InP) depicted in Fig. 2. Figure 1(a) gives the typical transverse electric [(TE)—electric field parallel to the holes] and transverse magnetic [(TM)—magnetic field parallel to the holes] band diagrams of a 2DPC having an air filling factor of 38%. For the calculation, we have taken into account the slab effective index value ($n_{\text{eff}} = 3.26$) of the TE-fundamental mode supported by the semiconductor heterostructure. Using these optogeometrical parameters, a “negative refraction regime” is achieved for the TE second band at reduced frequencies ranging from 0.23 to 0.36. In this range, the TM waves are reflected by a photonic band gap. This band exhibits a negative slope, while the wave vector isotropy is relatively preserved as shown by the circular isofrequency contours plotted in Fig. 1(b). Under these conditions [12], an effective negative index of $n = -1$ is achieved as the light line crosses this band which corresponds to a reduced frequency of $a/\lambda = 0.307$. Thus, for an operating wavelength of $1.55 \mu\text{m}$, the 2DPC lattice parameters are a 476 nm period with an air-hole diameter of 350 nm.

We then fabricated the flat lens by using the nanoelectronics techniques on III-V semiconductors [13]. The heterostructure is grown by molecular beam epitaxy, and the hole lattice is defined by *e*-beam lithography on a negative resist and then etched within the semiconductor slab by using the inductively coupled plasma etching technique. In addition, as depicted in Fig. 2(a), we also defined on the sample a monomode ridge waveguide terminated at a distance d from the lens input facet. This permits one to

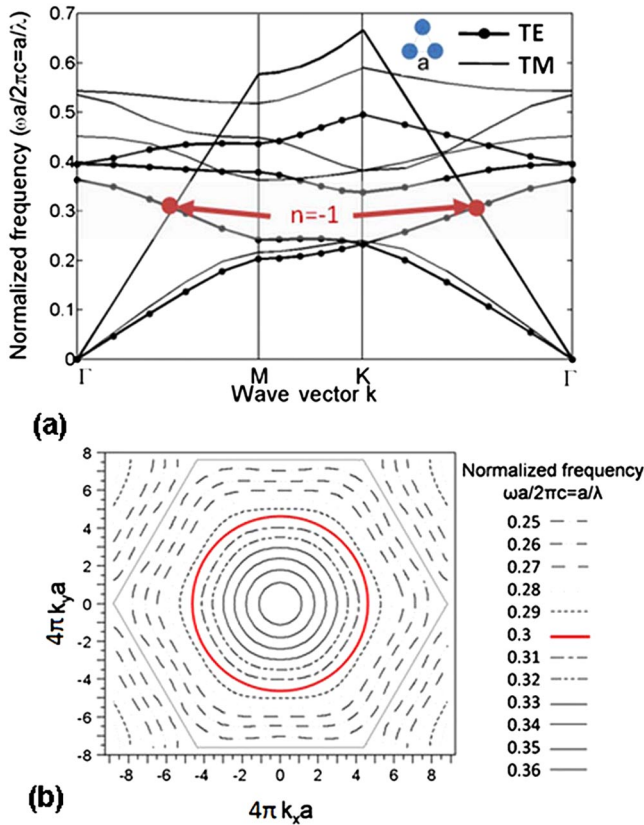


FIG. 1 (color online). (a) Band structure of TE (the electric field lies perpendicular to the 2D plane) and TM modes for a 2D triangular InP/InGaAsP air-hole triangular photonic crystal with an air filling factor of 38% and an effective index of 3.26. (b) Equifrequencies plot of the TE second band for the same photonic crystal.

generate a light source in the vicinity of the 2DPC flat lens that radiates a cylindrical wave front and mimics a sub-wavelength point source since the waveguide is $0.6 \mu\text{m}$ width with a high index contrast between air and the semiconductor limiting the spatial mode extension. At last, the distance d between the lens and the very end of the waveguide is chosen to $d = 4.5 \mu\text{m}$, which allows us to expect an intermediary focus point in the middle of the flat lens and an image spot at $2d_1 = 4d$ from the point source if the lens effective refractive index is $n = -1$. A scanning electron microphotograph (SEM) picture of the whole nanostructure is presented in Fig. 4(a).

Taking into account the geometrical parameters measured on the fabricated sample, we then computed by using a 3D finite-difference time-domain (FDTD) method the electromagnetic field intensity distribution within the whole device. Since, the lens design was performed in 2D, we found a 1% shift of the wavelength corresponding to $n = -1$ on the 3D calculations. In 3D, the $n = -1$ operating regime is rather achieved for an operating wavelength of 1525 nm. The 3D field distributions computed at this wavelength are plotted in Fig. 3. Figure 3(a) shows a

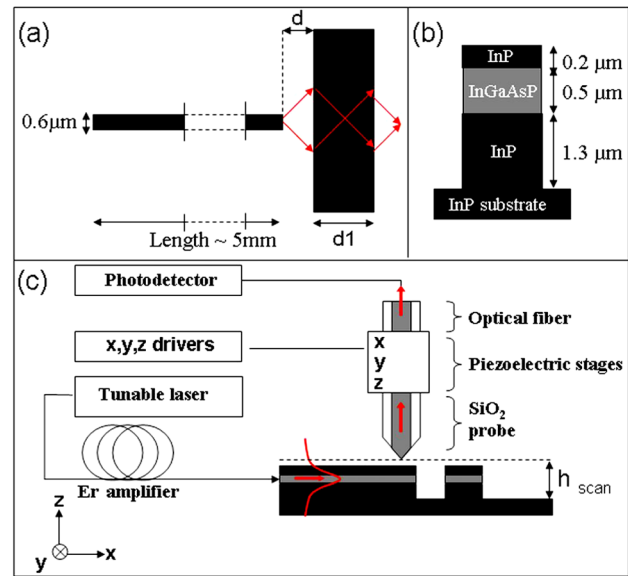


FIG. 2 (color online). Schematic view of (a) the structure with the rib waveguide and the 21st row ΓM -oriented photonic crystal lens ($d_1 = 9 \mu\text{m} = 2d$) and of (b) the InP-based heterostructure. (c) Schematic of the optical near-field experimental setup.

x - y cross section of the field intensity at the InGaAsP guiding layer height. It shows the focusing regime of the flat lens, the interference fringes related to the wave reflection at the lens input, and the field distribution within the 2DPC. We also plotted in Fig. 3(b) a x - z cross section of the field distribution along the middle of the structure. The

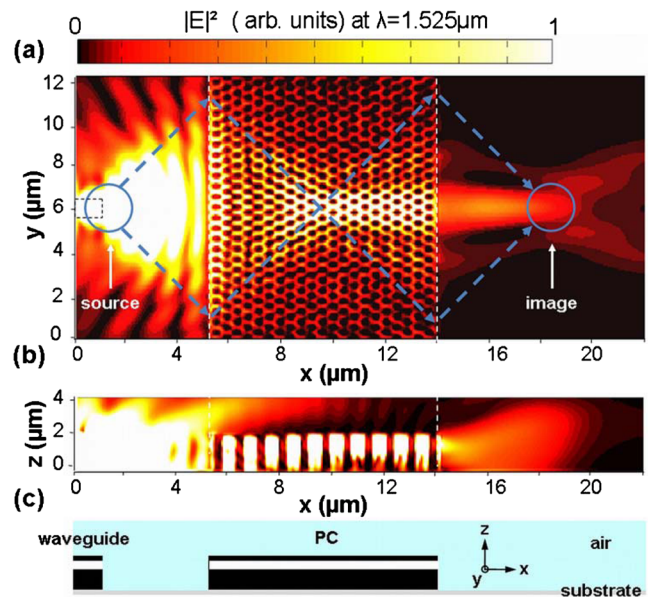


FIG. 3 (color online). Three-dimensional FDTD simulation of the focusing regime at 1525 nm: electric field intensity (a) in the xy plane ($z = 1.6 \mu\text{m}$ from the substrate corresponding to the InGaAsP layer) and (b) in the xz plane (middle of the ridge waveguide). The full device geometry is recalled in (c).

field vertical divergence in air and the out-of-plane losses in the ridge waveguide toward the substrate and at the lens interfaces can be clearly identified. More importantly, we observed that the ratio between transmitted and injected light is lower than 1%, which is not only due to diffraction in air at the ridge waveguide output but also to the imperfect impedance matching between incident waves in air and propagating waves inside the lens [14].

Next, the structure is characterized by a SNOM operating in collection mode. As depicted in Fig. 2(c), a TE polarized tunable laser source is injected inside the waveguide, while a near-field probe is scanned over the surface using piezoelectric stages. The distance between the probe and the surface is controlled by a shear-force feedback, and the SNOM pictures presented hereafter were recorded at a constant height scan [h_{scan} in Fig. 2(c)] of $2 \mu\text{m}$ from the substrate plane. The near-field probe consists in a chemically etched monomode silica fiber with a 100 nm-width apex which locally detects the electrical field intensity surrounding the nanostructure [15,16]. Moreover, since the near-field probes are generally more sensitive to the field components perpendicular to the probe axis and since the lens operates for a TE polarization of light, i.e., with a predominant electrical component parallel to the probe axis, the SNOM detection efficiency is very weak, and we used an Er amplifier to increase the input light power in order to improve the signal to noise ratio.

We recorded several SNOM pictures of the operating flat lens for wavelengths ranging from 1500 to 1600 nm. A bright spot at the lens output is observed for wavelength ranging from 1510 to 1540 nm, and its maximal visibility is achieved for an input wavelength of 1525 nm. The general SNOM picture corresponding to this wavelength is plotted in Fig. 4(b). An illuminated view is used since the observed features in the SNOM pictures have signal variations that differ by several orders of magnitude. We also note that, in

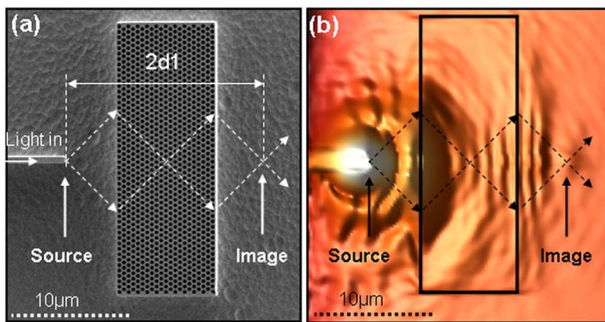


FIG. 4 (color online). (a) Scanning electronic microscope picture of the fabricated photonic crystal lens and the input waveguide that mimics a source point in the vicinity of the lens. (b) Scanning near-field optical microscope picture of the lens recorded for an input wavelength of $\lambda = 1525 \text{ nm}$. For a better visualization of the small amplitude signals that evidence the electromagnetic wave propagation inside the nanostructure, an illuminated picture is plotted.

Fig. 4, the SEM picture and the SNOM picture are plotted at the same scale to allow for a direct comparison. In the SNOM picture, from left to right, one can observe: (i) The end of the waveguide that mimics a point source and radiates a cylindrical wave front. The interference fringes observed around the waveguide termination correspond to the interference between the waves radiated by the waveguide and the waves reflected by the lens input facet. (ii) The wave propagation inside the 2DPC flat. The interference fringes resulting from the bouncing waves between the input and output facets of the flat lens are visible above the structure. (iii) The focalized spot appears on the SNOM picture as a bright localized spot at a distance $d = 4.5 \mu\text{m}$ from the lens output. (iv) A ray tracing corresponding to a $n = -1$ refractive index of the lens is superimposed on the SNOM picture and illustrates the focusing regime of the 2DPC flat lens. The distance between the source and its image is $2d_1$ as expected.

In light of these observations, one can now compare the evolution of the SNOM pictures recorded as a function of the wavelength (Fig. 5). The near-field patterns measured at the lens output clearly show the progressive appearance and disappearance of the image spot from 1510 to 1570 nm. It is also found that the image spot exists for a broad range of wavelengths from 1510 to 1540 nm, which is in good agreement with the isotropy of the equifrequency contours in this region and confirms the FDTD predictions presented in the first section of this Letter.

Finally, let us discuss and evaluate the reported lens ability to produce a subwavelength image of the source point. In order to evaluate the full width at half maximum (FWHM) of the focused spot, we used a Gaussian fit of the transverse cross section of the spots along the y direction. We found that, for wavelengths ranging from 1510 to 1540 nm, the spot FWHM values are dispersed between λ_0 and $1.2\lambda_0$. The optimal FWHM value λ_0 is measured in the case of the 1540 nm picture. This wavelength must correspond to the regime where $n = -1$ even if it does not

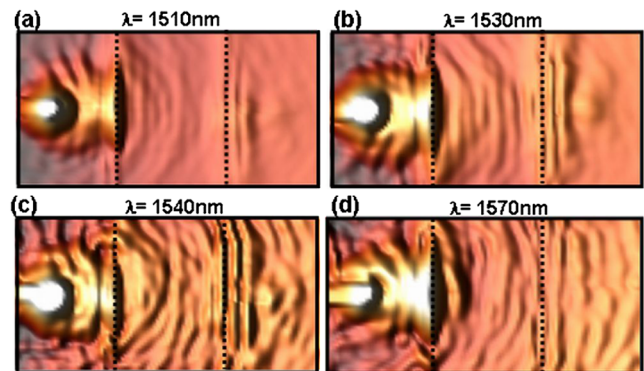


FIG. 5 (color online). SNOM pictures of the lens for different input wavelengths: (a) $\lambda = 1510 \text{ nm}$, (b) $\lambda = 1530 \text{ nm}$, (c) $\lambda = 1540 \text{ nm}$, and (d) $\lambda = 1570 \text{ nm}$. In each picture, the position of the lens facets is superimposed as dotted lines.

correspond to the brightest spot. However, if this measured value λ_0 at 1540 nm is not a subwavelength value, one needs to take into account the focused spot broadening due to the finite SNOM probe size [15,17]. As reported in our previous works on 2DPC structures [15,16], the probe induces a broadening of the field localization that can be approximated by a Gaussian function convolution. In the specific case of the probe we used in this work, the FWHM of the Gaussian is almost 250 nm. Consequently, after deconvolution, we estimated that the focused spot FWHM is $0.8\lambda_0$ in the better case. Consequently, even if the reported 2DPC flat lens seems to exhibit a subwavelength resolution to be compared to the one predicted by theorists [18] for such 2DPC nanostructures ($0.66\lambda_0$), one can notice that this does not permit one to conclude that the lens acts as a superlens breaking through the Rayleigh criterion ($0.5\lambda_0$).

This issue which still remains controversial may be discussed. If, on one hand, according to Pendry [2], “negative refraction makes a perfect lens,” recent considerations also suggest that the subwavelength resolution of 2DPC flat lenses may be mediated by a resonant coupling of surface waves [11,18,19] rather than by any amplification of evanescent waves. Consequently, achieving a super-resolution with a 2DPC flat lens not only requires one to take care of the negative refraction but also to consider the truncation of the PC. We note here that, on the presented SNOM images, the light detected at the lens interfaces mainly corresponds to out-of-plane diffracted waves rather than surface waves, and thus further improvements of the experimental setup are required to address the specific role of these surface waves in the reported experiment. On the other hand, addressing the issue of the superresolution of any lens ($<0.5\lambda_0$) also requires an ideal subwavelength source of propagative *as well as* evanescent waves, which is a numerical and experimental issue. As a matter of fact, in classical free space optics, such a source is diffractive [20], for example, a subwavelength hole milled into an opaque screen, but is not compatible with the integrated optics geometry. However, one can expect to overcome this limitation by using novel nondiffracting light source based on surface plasmons [21,22] or slot waveguides [23].

In conclusion, we demonstrated a two-dimensional photonic crystal lens operating at optical frequencies by directly measuring the light distribution inside the lens by using optical near-field microscopy techniques. We found that the focusing regime can be achieved over a 30 nm-wide spectral range and evaluated the lens ability to focus light at a subwavelength scale. We believe that this work is a significant step in the field of negative refraction and superlenses.

This work has received financial support from the Agence Nationale de la Recherche (ANR) under the FANI contract.

-
- [1] V.G. Veselago, Sov. Phys. Usp. **10**, 509 (1968).
 - [2] J.B. Pendry, Phys. Rev. Lett. **85**, 3966 (2000).
 - [3] G. Dolling, M. Wegener, C.M. Soukoulis, and S. Linden, Opt. Lett. **32**, 53 (2007).
 - [4] K. Aydin, I. Bulu, and E. Ozbay, Appl. Phys. Lett. **90**, 254102 (2007).
 - [5] D. Maystre and S. Enoch, J. Opt. Soc. Am. A **21**, 122 (2004).
 - [6] T. Decoopman, G. Tayeb, S. Enoch, D. Maystre, and B. Gralak, Phys. Rev. Lett. **97**, 073905 (2006).
 - [7] A. Berrier, M. Mulot, M. Swillo, M. Qiu, L. Thylen, A. Talneau, and S. Anand, Phys. Rev. Lett. **93**, 073902 (2004).
 - [8] E. Schonbrun, T. Yamashita, W. Park, and C. J. Summers, Phys. Rev. B **73**, 195117 (2006).
 - [9] T. Matsumoto, K. Eom, and T. Baba, Opt. Lett. **31**, 2786 (2006).
 - [10] Z. Lu, B. Miao, T.R. Hodson, C. Lin, J.A. Murakowski, and D.W. Prather, Opt. Express **15**, 1286 (2007).
 - [11] R. Moussa, S. Foteinopoulou, L. Zhang, G. Tuttle, K. Guven, E. Ozbay, and C.M. Soukoulis, Phys. Rev. B **71**, 085106 (2005).
 - [12] N. Fabre, X. Mélique, D. Lippens, and O. Vanbésien, Opt. Commun. (to be published).
 - [13] N. Fabre, S. Fasquel, C. Legrand, X. Mélique, M. Muller, M. François, O. Vanbésien, and D. Lippens, Opto-Electron. Rev. **14**, 225 (2006).
 - [14] C. Croenne, N. Fabre, D.P. Gaillot, O. Vanbésien, and D. Lippens, Phys. Rev. B (to be published).
 - [15] N. Louvion, D. Gérard, J. Mouette, F. de Fornel, C. Seassal, X. Letartre, A. Rahmani, and S. Callard, Phys. Rev. Lett. **94**, 113907 (2005).
 - [16] B. Cluzel, D. Gérard, E. Picard, T. Charvolin, F. de Fornel, and E. Hadji, J. Appl. Phys. **98**, 086109 (2005).
 - [17] P. Kramper, M. Kafesaki, C.M. Soukoulis, A. Birner, F. Müller, U. Gösele, R.B. Wehrspohn, J. Mlynek, and V. Sandogdhar, Opt. Lett. **29**, 174 (2004).
 - [18] C. Luo, S.G. Johnson, J.D. Joannopoulos, and J. Pendry, Phys. Rev. B **68**, 045115 (2003).
 - [19] R. Moussa, S. Foteinopoulou, L. Zhang, G. Tuttle, K. Guven, E. Ozbay, and C.M. Soukoulis, Phys. Rev. B **71**, 085106 (2005).
 - [20] E. Syngé, Philos. Mag. **6**, 356 (1928).
 - [21] M.I. Stockman, Phys. Rev. Lett. **93**, 137404 (2004).
 - [22] E. Verhagen, A. Polman, and L. Kuipers, Opt. Express **16**, 45 (2008).
 - [23] J.T. Robinson, S.F. Preble, and M. Lispon, Phys. Rev. Lett. **95**, 143901 (2005).